First hyperpolarizabilities of vinylogue organometallic sesquifulvalene chromophores: A DFT study

ARTICLE *in* INTERNATIONAL JOURNAL OF QUANTUM CHEMISTRY · OCTOBER 2006

Impact Factor: 1.43 · DOI: 10.1002/qua.21048

2 AUTHORS:

Chao-Yong Mang
Dali University
49 PUBLICATIONS **168** CITATIONS
SEE PROFILE

Kechen Wu
Chinese Academy of Sciences
154 PUBLICATIONS **1,485** CITATIONS
SEE PROFILE

First Hyperpolarizabilities of Vinylogue Organometallic Sesquifulvalene Chromophores: A DFT Study

CHAOYONG MANG, KECHEN WU

State Key Laboratory of Structural Chemistry, Fujian Institute of Research on the Structure of Matter, Chinese Academy of Sciences, Fuzhou, Fujian 350002, People's Republic of China

Received 15 June 2005; accepted 8 December 2005
Published online 5 April 2006 in Wiley InterScience (www.interscience.wiley.com).
DOI 10.1002/qua.21048

ABSTRACT: Static first hyperpolarizabilities of vinylogue mono- and bimetallic sesquifulvalene chromophores, $[(\eta^5\text{-}C_5H_5)M\{\mu\text{-}(\eta^5\text{-}C_5H_4)CH{=}CH(\eta^6\text{-}C_7H_7)\}]^+$ (M = Fe, Ru, and Os) and $[(\eta^5\text{-}C_5H_5)M\{\mu\text{-}(\eta^5\text{-}C_5H_4)CH{=}CH(\eta^6\text{-}C_7H_7)\}Cr(CO)_3]^+$ (M = Fe, Ru, and Os) have been calculated within DFT theoretical approach. The results agree well with the recent Hyper-Rayleigh scattering (HRS) measurements. The coordinated transition metals reduced the magnitude of dipole moment and first hyperpolarizability. The metal-to-ligand charge-transfer contributes to the first hyperpolarizability and, as a result, the rational substitution of coordinated metal could modulate the first hyperpolarizability of the organometallic chromophores. The study would be helpful to understand optical nonlinearities in organometallic complexes. Int J Quantum Chem 106: 2529–2535, 2006

Key words: sesquifulvalene; organometallic complexes; hyperpolarizability; electronic absorption spectra

Correspondence to: K. Wu; e-mail: wkc@fjirsm.ac.cn
Contract grant sponsor: National Science Foundation of China (NNSFC).
Contract grant number: 69978021.
Contract grant number: 20173064.
Contract grant number: 90203017.
Contract grant sponsor: Ministry of Science and Technology of China (MOST).
Contract grant number: 2004CB720605.

Introduction

The organometallic compound is an attractive field of nonlinear optical (NLO) material. The diverse molecular structures could be optimized for optimal nonlinear optical (NLO) activity with the aim at special applications in photonic devices [1–6]. Sesquifulvalene transition-metal compound is one of classes of organometallic compounds with large first hyperpolarizability. These compounds are typically composed of electron donors, electron acceptors and conjugated π-bridges offering the electronic communication between donor and acceptor. They are highly polarizable and exhibit the large second-harmonic generation (SHG) effects [7]. Heck and colleagues [8–11] reported a series of transition metal sesquifulvalene complexes with the large NLO response. They found that these organometallic complexes possessed the largest values of the first hyperpolarizabilities ever measured before. Theoretical investigations are essential to understand of the nature of NLO response of these complexes to perform molecular design for the new organometallics with the enhanced NLO effects.

The previous theoretical investigations on molecular organometallic NLO properties have mostly employed the semi-empirical quantum chemical methods [12–15], which have been remarkably successful in the understanding of optical nonlinearities of organometallics. For example, Kanis et al. [16] carried out a systemic study of the LO and NLO properties for some neutral organometallic ferrocenyl chromophores at ZINDO/sum-over-state (SOS) level. These investigators found that two energy bands characterized all the absorption spectra of these transition-metal chromophores. They pointed out that the low-energy (LE) transition was assigned to metal-localized ligand-field (*d-d*) transition which made little contribution to the first hyperpolarizabilities while the high-energy (HE) transition was subscribed as metal-to-acceptor transition with much contribution to the first hyperpolarizabilities.

In this study, we employed the first-principle quantum chemical methods to calculate the first hyperpolarizabilities of a series of organotransition metal chromophores. They are vinylogue sesquifulvalene μ−(η^5-C_5H_4)CH═CH(η^6-C_7H_7) (**1**) [17], vinylogue sesquifulvalene complex monocations, [(η^5-C_5H_5)M{μ–(η^5-C_5H_4)CH═CH(η^6-C_7H_7)}]$^+$ (M = Fe (**2**) [9], Ru (**3**) [10], Os (**4**)), and [(η^5-C_5H_5)M{μ−(η^5-C_5H_4)CH═CH(η^6-C_7H_7)}Cr(CO)$_3$]$^+$ (M = Fe (**5**) [8], Ru (**6**) [10], Os (**7**)).

The density functional theory (DFT) method is a feasible and reliable computational tool to calculate transition-metal containing systems with affordable computational resources. Some studies have reported the DFT theory, DFT applications, and DFT calculations on optical absorption spectra and the hyperpolarizability of organometallic compounds [18–36]. For example, Calaminici [37] evaluated the first hyperpolarizability of a ferrocenyl derivative.

The first hyperpolarizability is sensitive to many structural factors such as bond length [38], interplanar dihedral angles [39, 40] and the molecular distortion [41]. Our study on vinylogue transition metal sesquifulvalene ionic chromophores suggested that the substitution of coordinated transition metal could significantly change the first hyperpolarizability. The theoretical results agreed to the recent reported experiment measurement.

Computational Method

Figure 1 shows the structures of the organic vinylogue sesquifulvalene molecule (model **1**) and six transition-metal coordinated ionic chromophores (model **2–7**). Among them, **5–7** with two metal-coordinated fragments have the cissoid conformation and are located on the same side of the molecular plane of vinylogue sesquifulvalene. All the geometries of seven models were structural optimized without symmetry restriction at hybrid B3LYP functional [42, 43] and relativistic ECP basis set LanL2DZ [44, 45] level. The convergence criterion of SCF total energy was 10^{-8} a.u. and the threshold of the displacement vector was 0.001800 a.u.

The *x*-axis of model **1** is directed from cycloheptatrienyl ring to cyclopentadienyl ring. Similarly, the *x*-axes of model **2–7** are directed from the cyclopentadienyl to cycloheptatrienyl fragments. According to Kurtz's finite-field scheme [46], the components of the first static hyperpolarizability could be expressed by the following equations upon an external electric field F_i applied along the different coordination axes:

$$\beta_{iii} = \{[\mu_i(2F_i) + \mu_i(-2F_i)] - (1/3)[\mu_i(F_i) + \mu_i(-F_i)]\}/F_i^2 \quad (1)$$

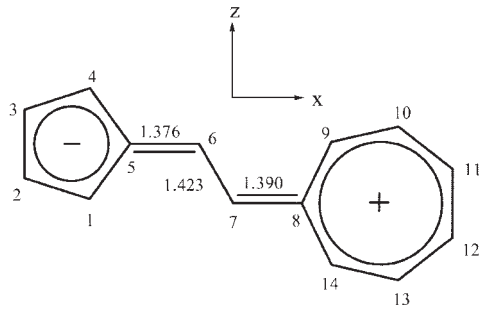

1

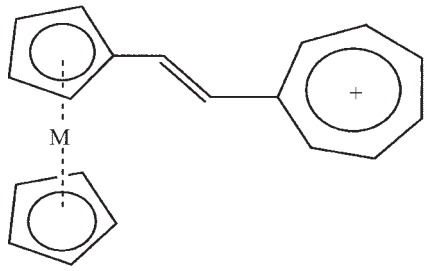

M = Fe (**2**); Ru (**3**); Os (**4**)

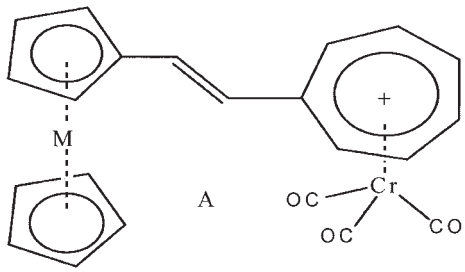

M = Fe (**5**); Ru (**6**); Os (**7**)

FIGURE 1. Molecular structure with orientation of the organic vinylogue sesquifulvalene $\mu-(\eta^5\text{-}C_5H_4)CH{=}CH(\eta^6\text{-}C_7H_7)$ (**1**), vinylogue monometallic sesquifulvalene chromophores $[(\eta^5-C_5H_5)M\{\mu-(\eta^5\text{-}C_5H_4)CH{=}CH(\eta^6\text{-}C_7H_7)\}]^+$ [M = Fe (**2**), Ru (**3**), and Os (**4**)], and vinylogue bimetallic sesquifulvalene chromophores $[(\eta^5\text{-}C_5H_5)M\{\mu-(\eta^5\text{-}C_5H_4)CH{=}CH(\eta^6-C_7H_7)\}Cr(CO)_3]^+$ [M = Fe (**5**), Ru (**6**), and Os (**7**)].

$$\beta_{ijj} = \{[\mu_i(2F_j) + \mu_i(-2F_j)] - (1/3)[\mu_i(F_j) + \mu_i(-F_j)]\}/F_j^2. \quad (2)$$

Recently, Calaminici [37] calculated the β values of a neutral ferrocenyl complex by using the gradient-corrected DFT method and found that the calculated values were in good agreement with the experimental data when the external-field intensity was 0.001 a.u. In our studies, $F_i = 0.001$ a.u was also adopted. The following relations were used to obtain the spatial average values of β [47]

$$\bar{\beta}^2 = \sum_i \beta_i^2 \qquad (i = x, y, z) \quad (3)$$

$$\beta_i = \beta_{iii} + \frac{1}{3}\sum_{i\neq j}(\beta_{ijj} + \beta_{jij} + \beta_{jji}) \qquad (i, j = x, y, z). \quad (4)$$

We used Debye as the unit of the dipole moment and the electrostatic unit (esu) for β, where 1 a.u. (atomic unit) = 0.008641×10^{-30} esu. The time-dependent DFT method was adopted to calculate the electronic excitation properties. The NLO natures of the models were analyzed by using the two-level approach. The electronic absorption spectrum of model **2** (Fig. 2) was simulated by Lorentz line-shape with a half-width of 30 cm^{-1}.

Results and Discussion

The optimized geometry parameters of seven models were listed in Table I, where θ represents the inter-planar rotational angle between the five- and seven-numbered rings. For model **2** and **5**, the optimized geometry parameters were in good agreement with the experimental measurement [8,

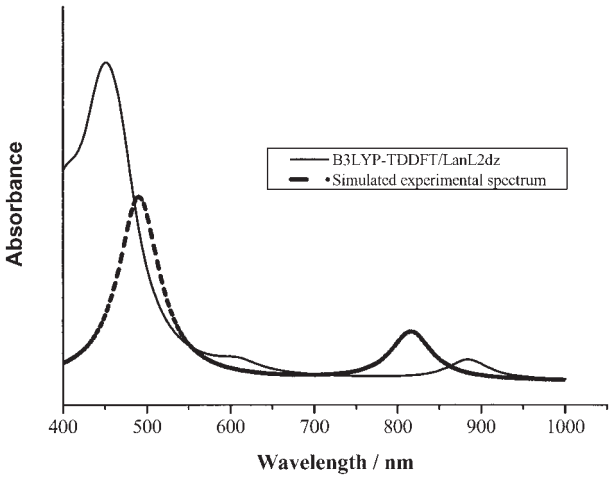

FIGURE 2. Simulated electronic absorption spectrum of both the calculated and experimental result of model **2**. The experimental values were taken from Ref. [9].

TABLE I

Optimized geometry parameters of model 1–7 at the B3LYP/LanL2DZ level.

	C_1—C_2	C_2—C_3	C_4—C_5	C_5—C_6	C_6—C_7	C_7—C_8	C_8—C_9	C_9—C_{10}	C_{10}—C_{11}	C_{11}—C_{12}	M—C_5	Cr—C_8	θ
1	1.378	1.477	1.474	1.376	1.423	1.390	1.465	1.373	1.452	1.372	—	—	0.0
2	1.429	1.446	1.430	1.431	1.387	1.438	1.464	1.442	1.430	1.388	2.125	—	8.4
Expt.[a]	1.405	1.394	1.423	1.460	1.310	1.452	1.398	1.362	1.391	1.376	2.042	—	1.69
3	1.434	1.449	1.465	1.430	1.389	1.436	1.444	1.388	1.431	1.387	2.282	—	9.5
4	1.443	1.451	1.471	1.432	1.389	1.436	1.444	1.388	1.431	1.387	2.265	—	10.8
5	1.428	1.447	1.464	1.427	1.390	1.430	1.452	1.408	1.436	1.407	2.129	2.586	4.9
Expt.[b]	1.428	1.390	1.413	1.462	1.347	1.439	1.423	1.393	1.400	1.413	2.046	2.358	7.2
6	1.433	1.449	1.466	1.426	1.393	1.426	1.453	1.407	1.436	1.407	2.275	2.601	5.8
7	1.441	1.451	1.471	1.428	1.393	1.425	1.453	1.406	1.437	1.407	2.261	2.604	5.3

[a] Data from Ref. [9] and bond lengths and angles are in Å and degrees, respectively.
[b] Data from Ref. [8].

9]. For instance, Fe—C_5 bonds of model **2** and **5** were 2.125 Å and 2.129 Å, respectively. These values were only about 0.083 Å longer than the corresponding experimental values. The structures of model **2** and **5** were twisted. The optimized θ values of models **2** and **5** were 8.4° and 4.9°, respectively. The measured data were 1.69° and 7.2°, respectively. We ascribed the larger deviation to the measured error that often occurs to such small angles. In fact, all the structures of the models were distorted due to the nonzero θ values. It is interesting that the optimized θ values of monometallic models were in the orders **2** (8.4°) < **3** (9.5°) < **4** (10.5°) and of bimetallic species, **5** (4.9°) < **6** (5.8°), **7** (5.3°). The heavier of the coordinated metal the larger the θ values were.

The conjugated π bridge in organic molecule **1** has the structure of C═CH—CH═C with the double-single-double carbo—carbon bond lengths being 1.376, 1.423, and 1.390Å, respectively. As a result, the ground state of model **1** has the characteristics of the cross-conjugated structure. However, the π-bridge of model **2–7** have the C—CH═CH—C conformation. For **2**, the single-double-single carbo—carbon bond lengths being 1.431, 1.387, and 1.438 Å (the corresponding experimental values are 1.460, 1.310, and 1.452 Å), respectively. And for model **5**, the optimized single-double-single bond lengths were 1.427, 1.390, and 1.430 Å (corresponding to the experimental data, 1.462, 1.347, and 1.439 Å), respectively. The variations of the carbon—carbon bonds between the two conjugated rings of models **2–7** are very small. This structural feature indicated that comparing to the vinylogue sesquifulvalene in free state, the vinylogue sesquifulvalene in a metal complex as a ligand has stronger conjugated characteristics. This variation in π bridge resulted in the larger first hyperpolarizability in metal-coordinated chromophores.

In Table I, M—C_5 lengths changed with the different M in a order of **2** (2.125 Å) < **3** (2.282 Å) ~ **4** (2.265 Å) and **5** (2.129 Å) < **6** (2.275 Å) ~ **7** (2.261 Å). While the total dipole moments (μ) varied in almost an opposite order of **2** (9.2D) > **3** (8.4D) ~ **4**(8.2D) and **5**(5.8D) > **6**(5.5D) ~ **7**(5.4D). The μ values of the bimetallic chromophores (models **5–7**) were much smaller than those of the monometallic ones. The electronic couplings between the two transition metals decrease the ground-state dipole moments.

The calculated β values of models **1–7** listed in Table II were all mainly determined by the β_{xxx} components indicating the dominant NLO polarization along the dipole moment direction. The calculated β values of models **3** and **5** agreed well with the recent HRS experimental data. For instance, the B3LYP results of the β values of model **3** are 95×10^{-30} esu agreed with the measured 105×10^{-30} and 120×10^{-30} esu [10]. For **5**, the β value was 115×10^{-30} esu which was close to the experimental value of 113×10^{-30} esu [8]. DFT methods are reliable for calculating the first hyperpolarizabilities containing transition-metal elements.

As we have mentioned, the geometry variations among the models affect the NLO response. The most important structural parameters to the property are M-C_5, Cr—C_8 andθ. The Fe—C_5 of model **2** is ~0.17 Å shorter than Ru—C_5 of model **3**. This resulted in about 14% increase of β in magnitude.

TABLE II

Calculated dipole moments μ (in D) and the static first hyperpolarizabilities β (in 10^{-30} esu) of model 1–7 at B3LYP/LANL2DZ level.

	1	2	3	4	5	6	7
μ_x	4.8	9.2	8.4	8.2	6.0	0.3[a]	0.0[b]
μ	4.8	9.2	8.4	8.2	5.8	5.5	5.4
β_{xxx}	22	103	91	88	98	76	72
β	21	108	95	92	115	89	85
Expt. β	—	—	120,[c] 105[c]	—	113[d]	59[c]	—

[a] Largest component is μ_z, 5.5 D.
[b] Largest component is μ_z, 5.4 D.
[c] Data from Ref. [10].
[d] Data from Ref. [8].

The similar situation could also be found for bimetallic chromophores (**5–7**). The stronger metal–ligand interaction could enhance the NLO response due to the enhancement of the electronic donor ability. It is obvious that the larger twist angle θ will restrain the conjugate characteristic. So it is reasonable to see that the larger θ the smaller β in magnitude for monometallic and bimetallic chromophores.

The calculated results showed that the β values of monometallic chromophores had a order of **2** (108) > **3** (95) > **4** (92) and the β values of the bimetallic species had a order of **5** (115) > **6** (89) > **7** (85). It is obvious that the β values decreased with the coordinated transition metals became heavier. This phenomenon makes it possible to tune the β magnitude by changing coordinated transition metal. However the further study is necessary for the in-depth understanding.

The LO parameters could be used to analysis the origin of NLO property by a simple scheme of the SOS expression [48, 49]. In many cases, only the first few excited states make a major contribution to the first hyperpolarizability. According to the two-level model [48–50], the first hyperpolarizability in magnitude upon charge transfer could be in the following simple expression:

$$\beta_{\mathrm{CT},x} = 6(\mu_{\mathrm{ex}} - \mu_x)\mu_x^2/E_{\mathrm{ge}}^2, \qquad (5)$$

where E_{ge} is the excited energy from the ground state to the charge-transfer excited state. μ_x and $(\mu_{\mathrm{ex}}-\mu_x)$ separately denote the transition dipole moment and the dipole-moment difference between the excited state and the ground state along the intramolecular charge-transfer direction (x). The μ_{ex} excitation dipole moment is difficult to obtain at present within DFT framework.

The electronic absorption spectrum of model **2** was simulated in Figure 2 by the calculated excitation transition frequencies and strengths at B3LYP/LanL2DZ level using the Lorentz line-shape modification. The calculated spectrum agreed well with the experimental one. The measured low-energy (LE) absorption peak at 816 nm corresponds to the calculated excitation transition at 884 nm. This transition was analyzed by the molecular orbital composition percentage. It came from the excitation from highest occupied molecular orbital (HOMO) to lowest unoccupied molecular orbital (LUMO). The orbital surfaces were displayed in Figure 3. The HOMO appeared to be mostly composed of $3d_{x^2-y^2}$ of Fe, and the LUMO was a delocalized π orbital of the ligands. The HOMO→LUMO excitation results in the intramolecular CT from the ferrocenyl group to the positively charged ligand. The metals to ligand CT (MLCT) make the major contribution to the NLO response of these organometallic chromophores. Although the coordinated metals of models **2–5**, Fe, Ru, and Os, belong to the same group in the Periodic Table, the first hyperpolarizabilities of these models were different. For example the replacement of Fe by Ru in models **2** and **5**, the first hyperpolarizabilities increased by 12% for **3** and 23% for **6** at the B3LYP/LanL2DZ level of computation. If Os replaced Fe, the increased percentages of β value were 15% for **4** and 26% for **7**.

The high-energy (HE) band at about 450 nm (measured data are at 490 nm) was composed of four calculated excited peaks at 468, 464, 446, and 440 nm. Among them the two strongest transitions at 464 and 446 nm were assigned to the excitations

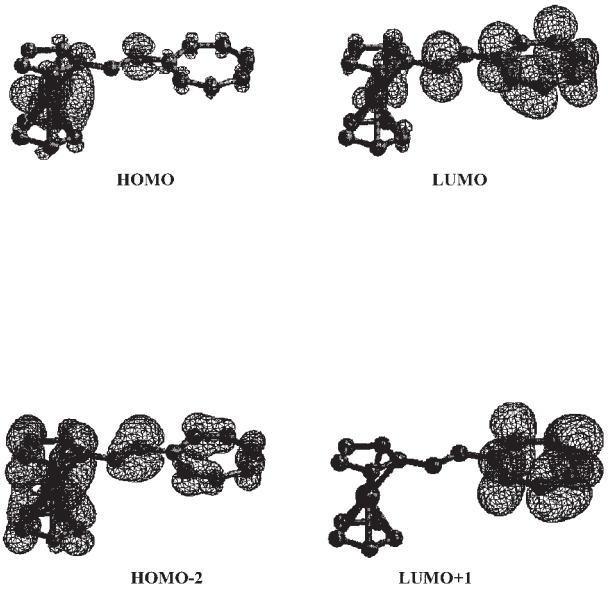

FIGURE 3. Molecular orbital surfaces represent the stable electron distributions of model **2**.

from HOMO-2 to LUMO+1. The frontier molecular orbital analysis showed that the HOMO-2 was a delocalized π orbital mainly populated on the five-numbered rings of the ferrocenyl group. The LUMO+1 was an unoccupied π^* orbital of the positively charged ligand. The HOMO-2→LUMO+1 excitation thus leads to the CT from the ligand of ferrocenyl group to the positively charged ligand. According to the two-level model, if μ_e—$\mu \neq 0$ the HE transitions could contribute to the first hyperpolarizability. In other words, the inter-ligand CT (ILCT) has some contributions to the first hyperpolarizability.

Conclusions

We report the DFT calculations on the first static hyperpolarizability of a series of vinylogue sesquifulvalene organometallic chromophores. The tunable first hyperpolarizabilities of these chromophores have been discussed. The first hyperpolarizabilities calculated at B3LYP/LanL2DZ level agreed well with the recent experimental data. The HOMO–LUMO transition implying the CT from the coordinated metal center to the substituent ligands (MLCT) contributes most to the first hyperpolarizability. It is thus feasible to modulate the molecular first hyperpolarizability by the substitute of the coordinated transition metal. We found in this study the possible tunable range up to 26% at B3LYP/Lanl2DZ level of theory. In addition, the HE inter-ligand CT (ILCT) contributed to the first hyperpolarizability as well. The heavier coordinated metal substitute might lead to larger molecular torsion and consequently decreased the dipole moment and the first hyperpolarizability. These results would be helpful to the understanding of the NLO origin of organometallics and the molecular design of organometallic chromophores for large hyperpolarizability.

References

1. Whittall, I. R.; MeDonagh, A. M.; Humphrey, M. G.; Samoc M. Adv Organomet Chem 1998, 42, 291.
2. Nalwa, H. S. Appl Organomet Chem 1991, 5, 349.
3. Bella, S. D. Chem Soc Rev 2001, 30, 355.
4. Verbiest, T.; Houbrechts, S.; Kauranen, M.; Klay, K.; Persoon, A. J. J Mater Chem 1997, 7, 2175.
5. Bozec, H. L.; Renouard, T. Eur J Inorg Chem 2000, 229.
6. Kanis, D. R.; Ratner, M. A.; Marks, T. J Chem Rev 1994, 94, 195.
7. Heck, J.; Dabek, S.; Meyer-Friedrichsen, T.; Wong, H. Coord Chem Rev 1999, 90-192, 1217.
8. Behrens, U.; Bussaard, H.; Hagenau, U.; Heck, J.; Hendrick, E.; Körnich, J.; Van Der Linden, J. G.; Persons, M. H.; Spek, A. L.; Veldman, N.; Voss, B.; Wong, H. Chem Eur J 1996, 2, 98.
9. Wong, H.; Meyer-Friedrichsen, T.; Farrell, T.; Mecker, C.; Heck, J. Eur J Inorg Chem 2000, 4, 631.
10. Meyer-Friedrichsen, T.; Wong, H.; Prosenc, M. H.; Heck, J. Eur J Inorg Chem 2003, 936.
11. Meyer-Friedrichsen, T.; Mecker, C.; Prosenc, M. H.; Heck, J. Eur J Inorg Chem 2002, 1, 239.
12. Bella, S. D.; Fragalà, I.; Marks, T. J.; Ratner, M. A. J Am Chem Soc 1996, 118, 12747.
13. Kanis, D. R.; Lacroix, P. G.; Ratner, M. A.; Marks, T. J. J Am Chem Soc 1994, 116, 10089.
14. Bella, S. D.; Fragalà, I.; Ledoux, P. G.; Zyss, J. Chem Eur J 2001, 7, 3738.
15. Bella, S. D.; Fragalà, I. Eur J Inorg Chem 2003, 2606.
16. Kanis, D. R.; Ratner, M. A.; Marks, T. J. J Am Chem Soc 1992, 114, 10338.
17. Babsch, H.; Prinzbach, H. Tetrahedron Lett 1978, 645.
18. Hieringer, W.; van Gisbergen, S. J. A.; Baerends, E. J. J Phys Chem A 2002, 106, 10380.
19. Gruning, M.; Gritsenko, O. V.; van Gisbergen, S. J. A.; Baerends, E. J. J Chem Phys 2002, 116, 9591.
20. van Gisbergen, S. J. A.; Guerra, C. F.; Baerends, E. J. J Comput Chem 2000, 21, 1511.
21. Champagne, B.; Perpete, E. A.; Jacquemin, D.; van Gisbergen, S. J. A.; Baerends, E. J.; Soubra-Ghaoui, C.; Robins, K. A.; Kirtman, B. J Phys Chem A 2000, 104, 4755.

22. Ricciardi, G.; Rosa, A.; van Gisbergen, S. J. A.; Baerends, E. J. J Phys Chem A 2000, 104, 635.
23. Schipper, P. R. T.; Gritsenko, O. V.; van Gisbergen, S. J. A.; Baerends, E. J. J Chem Phys 2000, 112, 1344.
24. van Gisbergen, S. J. A.; Snijders, J. G.; Baerends, E. J. J Chem Phys 1999, 111, 6652.
25. van Gisbergen, S. J. A.; Schipper, P. R. T.; Gritsenko, O. V.; Baerends, E. J.; Snijders, J. G.; Champagne, B.; Kirtman, B. Phys Rev Lett 1999, 83, 694.
26. van Gisbergen, S. J. A.; Snijders, J. G.; Baerends, E. J. Comput Phys Commun 1999, 118, 119.
27. Champagne, B.; Perpete, E. A.; van Gisbergen, S. J. A.; Baerends, E. J.; Snijders, J. G.; Soubra-Ghaoui, C.; Robins, K. A.; Kirtman, B. J Chem Phys 1999, 110, 11664.
28. van Gisbergen, S. J. A.; Snijders, J. G.; Baerends, E. J. J Chem Phys 1998, 109, 10644.
29. van Gisbergen, S. J. A.; Snijders, J. G.; Baerends, E. J. J Chem Phys 1998, 109, 10657.
30. van Gisbergen, S. J. A.; Kootstra, F.; Schipper, P. R. T.; Gritsenko, O. V.; Snijders, J. G.; Baerends, E. J. Phys Rev A 1998, 57, 2556.
31. van Gisbergen, S. J. A.; Snijders, J. G.; Baerends, E. J. Phys Rev Lett 1997, 78, 3097.
32. Jensen, L.; Duijnen, P. T. van; Snijders, J. G. J Chem Phys 2003, 119, 12998.
33. Chen, X. H.; Wu, K. C.; Snijders, J. G.; Lin, C. S. Chin Chem Lett, 2002, 13, 893.
34. Jensen, L.; Duijnen, P. T. van; Snijders, J. G.; Chong, D. P. Chem Phys Lett 2002, 359, 524.
35. Wu, K. C.; Chen, S. H.; Snijders, J. G.; Sa, R. J.; Lin, C. S.; Zhuang, B. T. J Cryst Growth 2002, 237, 663.
36. Wu, K.; Sa, R.; Lin, C. New J Chem 2005, 29, 362.
37. Calaminici, P. Chem Phys Lett 2003, 374, 650.
38. Meyers, F.; Marder, S. R.; Pierce, B. M.; Bréds, J. L. J Am Chem Soc 1994, 116, 10703.
39. Albert, I. D. L.; Marks, T. J.; Ratner, M. A. J Am Chem Soc 1997, 119, 3155.
40. Albert, I. D. L.; Marks, T. J.; Ratner, M. A. J Am Chem Soc 1998. 120, 11174.
41. Lin, C.; Wu, K.; Sa, R.; Mang, C.; Liu, P.; Zhuang, B. Chem Phys Lett 2002, 363, 343.
42. Lee, C.; Yang, W.; Parr, R. G. Phys Rev B 1988, 37, 785.
43. Becke, A. D. J Chem Phys 1993, 98, 5648.
44. Hay, P. J.; Wadt, W. R. J Chem Phys 1985, 82, 270, 284 and 299.
45. Dunning, T. H., Jr.; Hay, P. J. Modern Theoretical Chemistry; Vol III; Schaefer, H. F., Ed.; Plenum: New York, 1976.
46. Kurtz, H. A.; Stewart, J. P.; Dieter, M. J Comput Chem 1990, 11, 82.
47. Bishop, D. M. Advances in Chemical Physics; Vol 104; Prigogime, I.; Rice, S. A., Eds. John Wiley & Sons: New York, 1998.
48. Oudar, J. L.; Chemla, D. S. J Chem Phys 1977, 66, 2664.
49. Meyers, F.; Marder, S. R.; Pierce, B. M.; Breads, J. L. J Am Chem Soc 1994, 116, 10703.
50. Zyss, J.; Brasselet, S.; Thalladi, V. R.; Desiraju, G. R. J Chem Phys 1998, 109, 658.